Journal of
MATERIALS RESEARCH

Synthesis of nanocrystalline manganese oxide powders: Influence of hydrogen peroxide on particle characteristics

Jooho Moon, Masanobu Awano, Hiroyoshi Takagi, and Yoshinobu Fujishiro
National Industrial Research Institute of Nagoya, Nagoya 462, Japan

(Received 14 August 1999; accepted 2 September 1999)

Nanocrystalline manganese oxide powders have been prepared at 25 °C by precipitation from $Mn(NO_3)_2$ aqueous solution. The presence and addition sequence of H_2O_2 significantly influence particle characteristics of the resulting manganese oxides, including crystal structure, particle size and morphology, and surface area, depending upon molar ratio of H_2O_2 with respect to Mn. The precipitation from preoxidized manganese solution by H_2O_2 results in flakelike-shaped amorphous hydrous manganese oxide ($MnO_2 \cdot xH_2O$). In the absence of H_2O_2, on the other hand, amorphous $Mn(OH)_2$ is obtained, and a part of $Mn(OH)_2$ subsequently transforms into crystalline Mn_3O_4 by oxidation in air. Relative population of amorphous $Mn(OH)_2$ decreases by dissolution when post-treated with H_2O_2. At $Mn:H_2O_2 = 1:4$, the well-defined 16-nm-sized nanocrystalline Mn_3O_4 with homogenous particle morphology is prepared. The treatment with excess H_2O_2, however, destroys crystalline Mn_3O_4 and leads to further oxidation of the aqueous manganese species. Under these conditions, a mixture of needlelike Mn_2O_3 and cubelike Mn_3O_4, including amorphous $MnO_2 \cdot xH_2O$, is obtained.

I. INTRODUCTION

Manganese oxides are technologically important materials with a variety of applications. They have been used as oxidative catalysts, electrode materials for rechargeable lithium batteries, starting materials in ferrite production, and colorants and corrosion inhibiting agents for paints.[1–4] Recent research also demonstrated that ultrafine manganese oxides can be utilized as an abrasive in chemical mechanical polishing (CMP).[5,6] Hanawa *et al.* reported that the manganese oxides behave similarly as CeO_2 in the CMP process of Si and SiO_2.[7] Even for metals such as W or Cu, the enhanced polishing effect was observed owing to oxidation capability of the manganese oxides.

Another advantage of the manganese oxide in the CMP process is its ease for cleaning. In general, various foreign contaminants including abrasives, metals, and chemicals are introduced to a wafer to aid rapid polishing during the CMP processing. Post-CMP cleaning of these contaminants is thus a key step in successful CMP processing. The typical method involves a combination of chemical cleaning, ultrasonic cleaning, and mechanical brush scrubbing.[8] However, the particles adhere to polished surfaces by strong intermolecular forces such as van der Waals force and electrostatic double layer interaction. The removal of such particulate materials often poses a significant challenge in both practical and technological aspects. In contrast, the manganese oxides are usually stable in acidic solution but become readily soluble below pH 6 in the presence of reducing agents.[7] This unique dissolution behavior makes the manganese oxides easily cleaned after polishing without applying external forces.

Significant research has been conducted on the preparation of both porous and dense manganese oxides, which includes sol-gel, precipitation, hydrothermal, and solid-state reactions[9–12]. For instance, various fine manganese oxides (MnO, Mn_2O_3, Mn_3O_4, MnO_2) were synthesized by precipitation of manganese salts followed by calcination at temperatures ranging from 300 to 650 °C.[13–16] Reduction of $KMnO_4$ by either precipitation, hydrothermal, solvothermal, γ-ray radiation, or sonochemical reactions can produce both mesoporous and dense crystalline manganese oxides.[11,12,17–19] Electrolytic oxidation of $MnSO_4$ at the cathode has also been widely used to synthesize MnO_2 for dry cells.[20] These previous chemical syntheses have usually produced the manganese oxides with improved characteristics. However, most of methods are cost ineffective and cannot lead to uniform nanocrystalline particles.

In the present study, nanocrystalline manganese oxides with controlled particle size and shape are prepared by precipitation of manganese nitrate solution at room temperature followed by drying at 120 °C. The resulting solids show different phases, crystallinities, and particle morphologies depending upon synthesis procedure. Spe-

cial emphasis is directed onto studying the roles of hydrogen peroxide on the particle characteristics of the synthesized manganese oxides.

II. MATERIALS AND METHOD

Various manganese oxides were prepared by varying synthesis conditions. $Mn(NO_3)_2 \cdot 6H_2O$ (Wako Chemicals, 98%) was used as a precursor. Preliminary study indicated that other manganese salts such as sulfate, chloride, and acetate resulted in similar manganese oxides, but the nitrate salt gave rise to the most well-defined manganese oxides. First of all, manganese nitrate was dissolved in deionized water. The standard concentration of aqueous manganese solution was 0.3 M. Manganese hydroxide was precipitated at room temperature by addition of NH_4OH. The pH of the precipitate suspension was around 9.5.

The precipitation was also achieved in the presence of hydrogen peroxide to control the oxidation state of the manganese species. Hydrogen peroxide was introduced in two different ways. H_2O_2 was added either to manganese nitrate solution prior to precipitation or to the suspensions of the precipitated manganese oxides. The amount of H_2O_2 added was also varied from a molar ratio of $Mn:H_2O_2 = 1:1$ to 1:10 to study its influence on the particle characteristics of the manganese oxides.

After precipitation and post-treatment with H_2O_2, the resulting solids were aged at 25 °C for 1 h under rigorous stirring. The precipitates were then recovered by repeated washing and decantation to remove undesired impurity species. The recovered solids were dried in an oven at 120 °C for 18 h.

The phase of the manganese oxides was characterized by X-ray diffraction (XRD, Phillips APD1700). Thermal stability was also studied in air at a rate of 10 °C/min using thermogravimetric differential thermal analysis (TG-DTA, Rigaku, Thermoplus TG8120). The particle characteristics such as particle morphology and specific surface area were analyzed by transmission electron microscopy (TEM, JEOL JEM-4000FX) and Brunauer–Emmett–Teller analysis (BET, Coulter, Omnisorp 360), respectively.

III. RESULTS

The presence of hydrogen peroxide and its addition sequence result in significant differences in properties of the manganese precipitates. Particle characteristics of the manganese oxides prepared in the present study are summarized in Table I. Neutralization of manganese nitrate solution in the absence of H_2O_2 gave rise to brown precipitates (sample CMP06). Precipitation from hydrogen peroxide added manganese solution ($Mn:H_2O_2 = 1:1$ in molar ratio), on the other hand, produced black solids (sample CMP01).

Post-treatment with H_2O_2 produces different results depending upon the conditions at which the manganese oxides are prepared. Addition of the hydrogen peroxide to a suspension of the precipitates obtained from the H_2O_2 present solution (sample CMP01) prior to washing and drying did not cause any significant reaction. When H_2O_2 was introduced to the precipitates prepared in the absence of H_2O_2 (sample CMP06), however, vigorous exothermic reaction accompanied with evolution of gas occurred. The brown color of the precipitates turned into black as the amount of H_2O_2 increased (from sample CMP02 to CMP05).

XRD analysis indicated as shown in Fig. 1 that brown precipitates were γ–Mn_3O_4 (hausmanite), whereas black precipitates were amorphous hydrous manganese oxide with a minor phase of $(NH_3)_2Mn_8O_{16}$. It should be noted that x-ray reflection patterns for γ–Mn_3O_4 (JCPDS 24-0734) and γ–Mn_2O_3 (JCPDS 18-0803) are very similar, but they can be distinguished by comparing relative intensities for the first 6 peaks.

H_2O_2 post-treatment of the sample CMP01 did not give any change in phase composition as compared to the untreated one. For the manganese oxides prepared in the absence of H_2O_2, post-treatment alters to a great extent

TABLE I. Summary of the characteristics of the synthesized manganese oxides.[a]

	Sample ID					
	CMP01	CMP02	CMP03	CMP04	CMP05	CMP06
$Mn:H_2O_2$ ratio	1:1	1:1	1:4	1:7	1:10	N/A[c]
Order of addition	before ppt[b]	after ppt	after ppt	after ppt	after ppt	
Color of powders	Black	Chocolate brown	Black	Black	Black	Brown
Major phase	Amorphous	Mn_3O_4	Mn_3O_4	Mn_3O_4	Amorphous	Mn_3O_4
Minor phase	$(NH_3)_2Mn_8O_{16}$			Mn_2O_3	Mn_3O_4, Mn_2O_3	
Surface area (m^2/g)	100.1	25.3	46.1	49.2	51.2	23.4

[a]All the powders were prepared at room temperature followed by drying at 120 °C for 18 h.
[b]ppt: precipitation.
[c]N/A: not applicable.

the crystal structure of the synthesized manganese oxides. Crystallinity of Mn_3O_4 decreased with an increasing amount of H_2O_2 as shown in Fig. 2. ϵ–Mn_2O_3 (pyrolusite) was observed as a minor phase when excess hydrogen peroxide above the molar ratio of $Mn:H_2O_2$ = 1:7 was used in the post-treatment process. A mixture of Mn_3O_4 and ϵ–Mn_2O_3 with reduced crystallinity was detected in the sample CMP05.

Figure 3 shows the results of TG-DTA analysis for various manganese oxide powders. The samples CMP06 and CMP02 slightly gained weight up to ~500 °C after initial weight loss. In contrast, the samples CMP01 and CMP05 lost their weight gradually, followed by abrupt loss at 525 °C. All the manganese oxides underwent phase transformation twice at ~525 and 945 °C, accompanying endothermic reactions. Weight loss at low temperatures is attributed to removal of structural water. Weight gain observed in both samples CMP06 and CMP02 is supposedly due to oxidation of the manganese oxides with lower valence Mn^{2+} species to those with higher valence. X-ray analysis indicated that high-temperature-calcined samples for all the synthesized manganese oxides at 600 °C were Mn_2O_3 (bixbyite-C, JCPDS 41-1442), and the samples calcined at 1000 °C was Mn_3O_4 with a minor phase of Mn_2O_3, as shown in Fig. 1.

Surface area of the powders is a function of H_2O_2. Surface areas of amorphous manganese oxide (CMP01) and Mn_3O_4 (CMP06) were 100.1 and 23.4 m^2/g, respectively. Variation of hydrogen peroxide concentration from 1:1 to 1:7 in a molar ratio during post-treatment

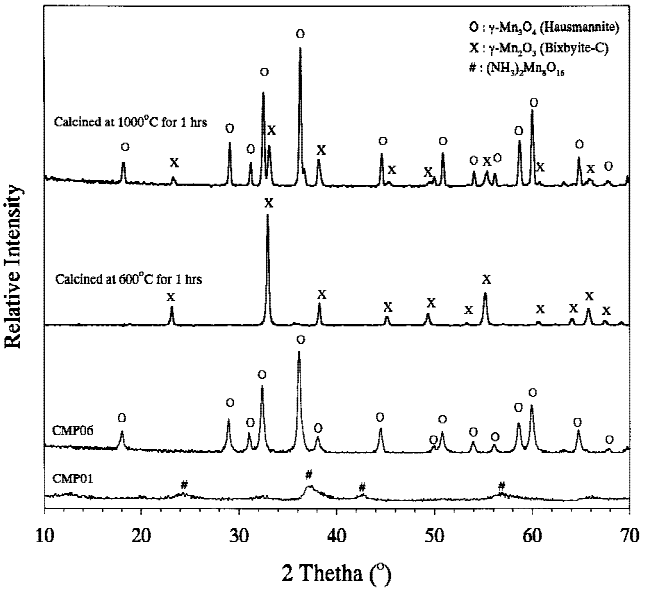

FIG. 1. X-ray diffraction patterns for the synthesized and calcined manganese oxides.

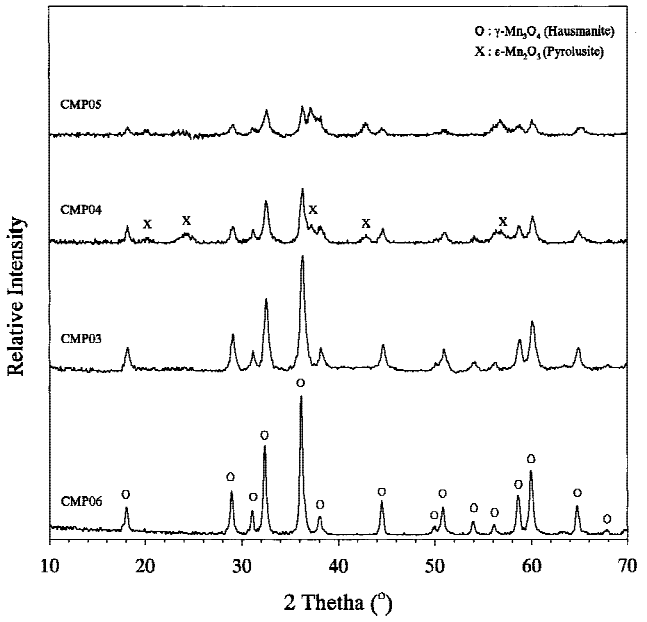

FIG. 2. X-ray diffraction patterns of manganese oxides as a function of H_2O_2 post-treatment.

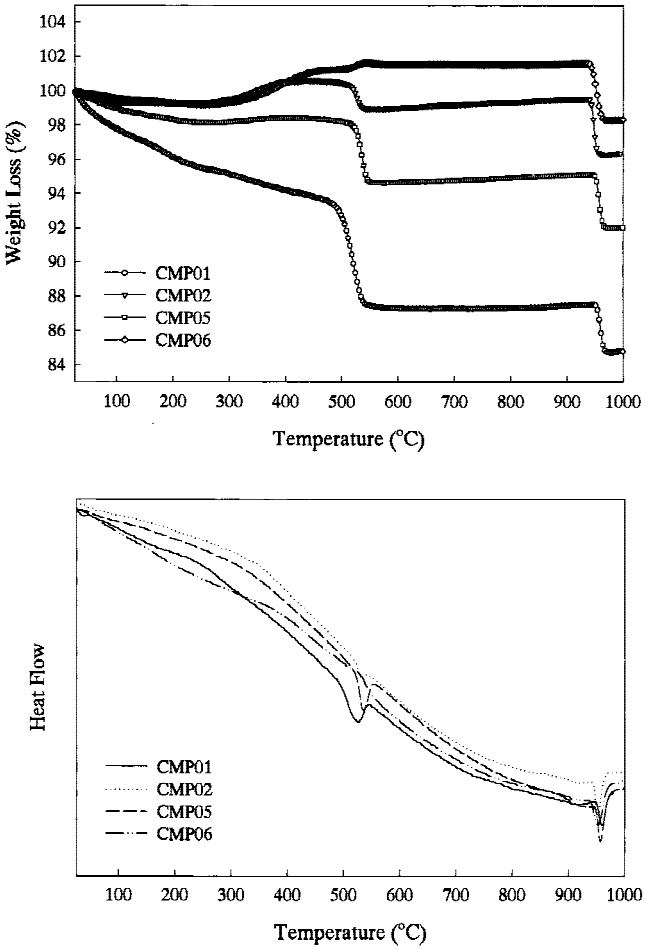

FIG. 3. TG-DTA curves for the various manganese oxides.

increased the surface area of the resulting manganese oxides from 25.3 to 49.2 m^2/g. Further addition of H_2O_2 above 1:7 did not involve significant change in surface area.

Particle morphologies of the synthesized manganese oxides are also different depending upon synthesis procedure. Amorphous manganese oxide (CMP01) has a flakelike shape, and its particle size is in the range 30–50 nm in length, as shown in the TEM micrograph of Fig. 4(a). On the other hand, the sample CMP06 is a mixture of cubelike particles of size ~14 nm and relatively spherical particles of ~80 nm [Fig. 4(b)]. On the basis of analyses of selected area diffraction by TEM and x-ray, the smaller particles are crystalline Mn_3O_4 and the larger precipitates are amorphous $Mn(OH)_2$. When hydrogen peroxide was introduced after precipitation, larger amorphous particles disappeared and the number of crystalline Mn_3O_4 increased [Fig. 4(c)]. At a molar ratio of $Mn:H_2O_2 = 1:4$, only the well-defined cubelike Mn_3O_4 were monitored as presented in Fig. 4(d). Particle morphology was homogeneous, and no other shape was detected. The average particle size of the sample CMP03 is approximately 16 nm.

Upon further addition of H_2O_2, the average sizes of cubelike particles become larger (~21 nm) and a few needle-shaped particles with much higher aspect ratio are also present [Fig. 4(e)]. It is believed that needle-shaped particles are ϵ–Mn_2O_3 according to analyses of x-ray (Fig. 2) and TEM. The sample CMP05 displays both larger irregular-shaped and needle-shaped particles, and the number of needle-shaped particles increases as shown in Fig. 4(f).

IV. DISCUSSION

In manganese oxides, the cations exist in multiple oxidation states (Mn^{2+}, Mn^{3+}, and Mn^{4+}), and the oxides exhibit high structural complexity with a wealth of metastable polymorphs.[21] Numerous studies concerning various aspects of the manganese oxide system have been

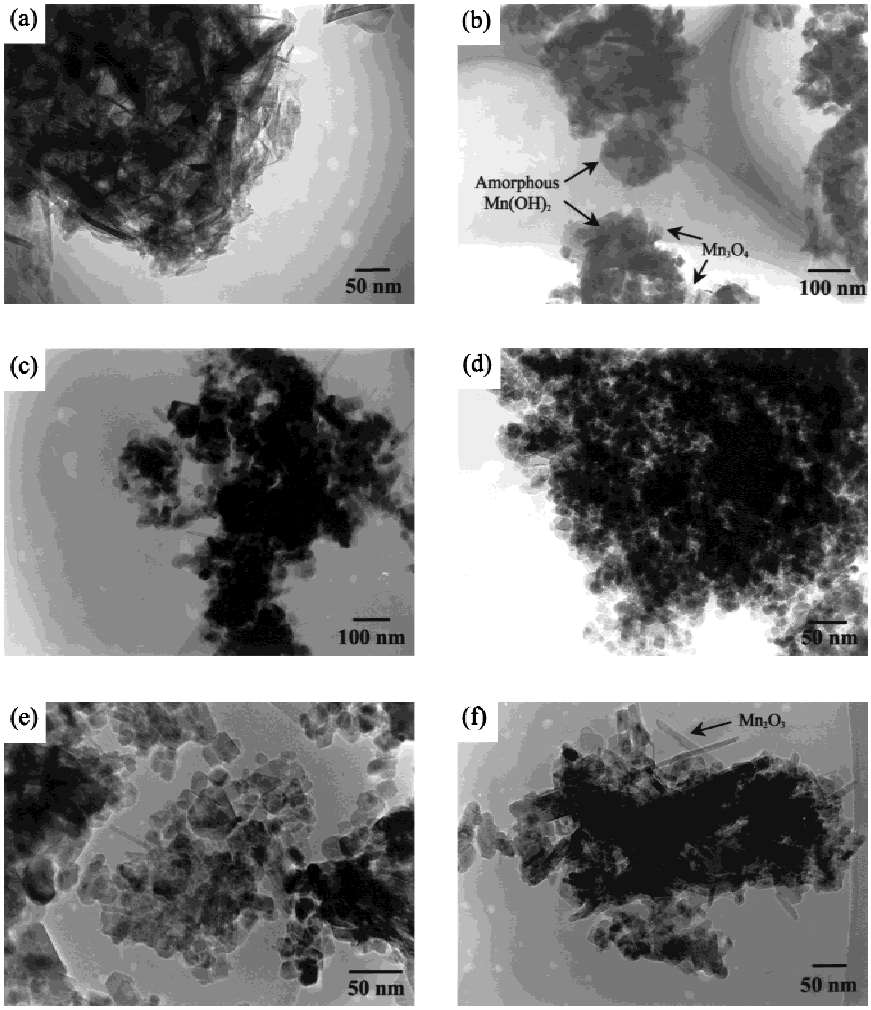

FIG. 4. TEM micrographs of the manganese oxides: (a) CMP01, (b) CMP06, (c) CMP02, (d) CMP03, (e) CMP04, (f) CMP05.

reported. In particular, γ–Mn_3O_4 occurs in nature as the mineral hausmannite in a distorted tetragonal spinel structure. The unit cell contains $Mn_4Mn_8O_{16}$ in which the O atoms are closed packed with Mn^{2+} ion in the tetrahedral site and Mn^{3+} in the octahedral site.[19]

Neutralization of manganese nitrate solution in alkaline conditions in the absence of hydrogen peroxide results in rapid precipitation of Mn^{2+} species. The color of the resulting solids is light brown when precipitated and turns into dark brown when aged. It is believed that hydrolysis of Mn^{2+} gives rise to amorphous $Mn(OH)_2$ according to the Eq. (1). A part of this precipitate can undergo oxidation in air as described below, which causes a change of color.[22,23]

$$Mn^{2+} + 2OH^- \rightarrow Mn(OH)_2 \quad (1)$$

$$4Mn(OH)_2 + O_2 + 2H_2O \rightarrow 4Mn(OH)_3 \quad (2)$$

The precipitates from aqueous manganese solution thus consist of amorphous $Mn(OH)_2$ and amorphous $Mn(OH)_3$. As shown in Fig. 5, the manganese oxides in the very early stage that were collected at 2 min after precipitation at 25 °C without drying have an open amorphous structure.

Aging of these precipitates leads to further oxidation in air, resulting in crystallization of Mn_3O_4 [Eq. (3)]. It is considered, however, that aging and drying at 120 °C are not sufficient to oxidize all the $Mn(OH)_2$, and the precipitation in the absence of H_2O_2 produces the mixed manganese oxides of crystalline Mn_3O_4 and amorphous $Mn(OH)_2$ as present in Fig. 4(b).

$$Mn(OH)_2 + 2Mn(OH)_3 \rightarrow Mn_3O_4 + 4H_2O \quad (3)$$

When hydrogen peroxide is added to an aqueous manganese solution, on the other hand, Mn^{2+} is oxidized to Mn^{4+} as shown in Eq. (4). Hydrolysis of Mn^{4+} may result in amorphous hydrous $MnO_2 \cdot xH_2O$ [Eq. (5)]. The existence of the impurity phase, $(NH_3)_2Mn_8O_{16}$, in the sample CMP01 supports that H_2O_2 effectively converts the oxidation state of the manganese aqueous species from +2 to +4 as shown below.

$$Mn^{2+} + H_2O_2 + 2H^+ \rightarrow Mn^{4+} + 2H_2O \quad (4)$$

$$Mn^{4+} + xH_2O + 2OH^- \rightarrow MnO_2 \cdot xH_2O + 2H^+ \quad (5)$$

When H_2O_2 is introduced to the manganese oxides after precipitation, it can oxidize the lower valence manganese species located in both crystalline and amorphous solids accompanying violent endothermic reactions according to the following reactions:[24]

$$>Mn^{2+} + H_2O_2 \leftrightarrow >Mn^{3+} + OH^- + OH^{\cdot} \quad (6)$$

$$>Mn^{2+} + OH^{\cdot} \leftrightarrow >Mn^{3+} + OH^- \quad (7)$$

$$H_2O_2 + OH^{\cdot} \leftrightarrow H_2O + HO_2^{\cdot} \quad (8)$$

$$HO_2^{\cdot} \leftrightarrow H^+ + O_2 \quad (9)$$

$$H_2O_2 + O_2 \leftrightarrow OH^- + OH^{\cdot} + O_2 \quad (10)$$

where > indicates surface-bound species. This reaction cycle is terminated when the last radicals produced in Eq. (10) are consumed in Eq. (7). The evolved oxygen also enhances oxidation, and the pH of the medium increases. The absence of such oxidation reactions when H_2O_2 is added to amorphous $MnO_2 \cdot xH_2O$ (CMP01), however, indicates that H_2O_2 is ineffective as an oxidizing agent since the valence of the manganese species already reaches +4.

It can be speculated that H_2O_2 preferentially attacks amorphous $Mn(OH)_2$ as compared to Mn_3O_4 due to its lower crystallinity and open structure. As presented in pictures from Figs. 4(c) to 4(f), the particle morphologies of the manganese oxides undergo gradual modification depending upon the amount of H_2O_2 added. Larger spherical amorphous $Mn(OH)_2$ disappears continuously due to its dissolution with the increasing amount of oxidation agent H_2O_2. Dissolved $Mn(OH)_2$ transforms into crystalline Mn_3O_4 under this oxidizing atmosphere. At the condition of $Mn:H_2O_2 = 1:4$, cubelike nanocrystalline Mn_3O_4 with uniform particle shape is obtained. Such additional particle nucleation and growth of Mn_3O_4 led to an increase in the average particle size of Mn_3O_4 from 14 to 21 nm as shown in TEM micrographs from Figs. 4(c) to 4(e).

When the amount of H_2O_2 exceeds a limit that is sufficient for dissolution and oxidation of all the amorphous $Mn(OH)_2$, further oxidation of the aqueous manganese species from +3 to +4 may occur, and even the crystalline structure of Mn_3O_4 could be destroyed as indicated by reduction in x-ray intensity in Fig. 2. In the excess H_2O_2 conditions, needlelike Mn_2O_3 reprecipitates from the so-

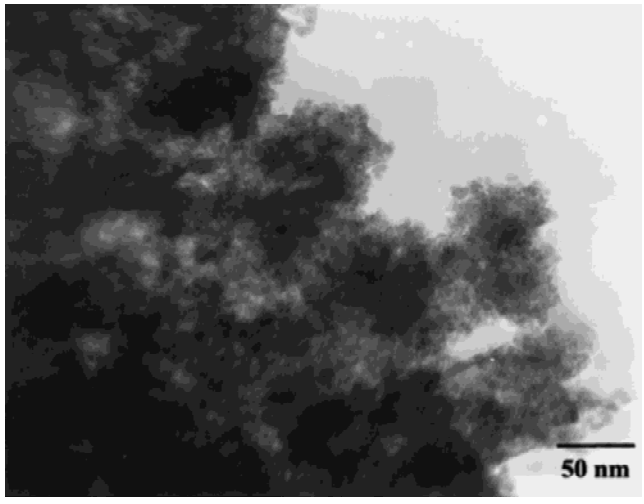

FIG. 5. TEM micrograph of the as-precipitated manganese oxide in the absence of H_2O_2. The sample was collected and prepared 2 min after precipitation at 25 °C.

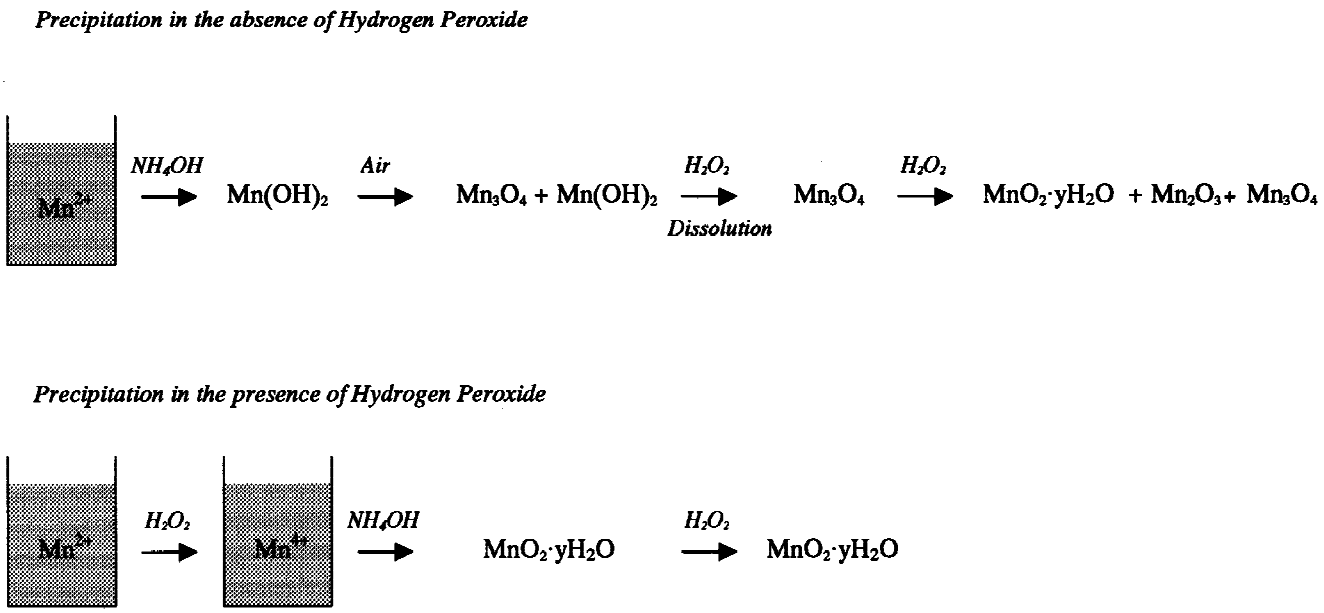

FIG. 6. Schematic picture illustrating formation mechanism of the manganese oxides.

lution of oxidized manganese species. TEM pictures [Figs. 4(e) and 4(f)] show increased population of needlelike Mn_2O_3 and decreased number of cubelike Mn_3O_4 with the increasing H_2O_2. The formation mechanism of various manganese oxides depending upon the synthesis scheme is schematically illustrated in Fig. 6.

To verify dissolution behavior of $Mn(OH)_2$ by H_2O_2, Mn_3O_4 was prepared at three different precursor concentrations (0.1, 0.2, and 0.4 M) followed by post-treatment with H_2O_2 at the identical molar ratio ($Mn:H_2O_2 = 1:4$). If our hypothesis is valid, the particle size of the resulting manganese oxides should depend on the precursor concentrations. Concentrated conditions can set up higher supersaturation of dissolved Mn solution, from which a greater number of nuclei can form and grow rapidly, resulting in smaller particle sizes. At less concentrated conditions, on the other hand, the driving force for nucleation is relatively low and the dissolved species reprecipitate on the pre-existing Mn_3O_4, making particle size larger. As presented in Fig. 7, the particle sizes of the manganese oxides decrease with an increasing precursor concentration from approximately 32 to 13 nm as predicted. The particle morphologies are somewhat elongated rectangular shape at 0.1 M, whereas the equiaxed particles are observed at 0.4 M. It should noted here that secondary nucleation and growth generally lead to a wider distribution of particle size. It is expected, however, that the rate of nucleation is sufficiently faster than the rate of growth, allowing relatively uniform particle distributions in the current system.

Different thermal stability of the manganese oxides can also be understood from the details of the influence of H_2O_2 post-treatment on the particle characteristics. In lower temperature ranges, all the samples lose their coordinated waters as shown in Fig. 3. Further thermogravimetrical behavior depends upon the phase and its relative composition existing in the mixed manganese oxides. The samples that contain the manganese oxides of oxidation state lower than +4 show gradual weight gain after $T > 200$ °C due to oxidation. The difference in the amount of weight gain in the samples from CMP02 to CMP06 implies that the relative ratio of Mn^{2+}, Mn^{3+}, and Mn^{4+} in the manganese oxides is modified by H_2O_2 post-treatment. With the increased amount of H_2O_2, the oxidized Mn species increase, and less weight gain is observed as shown in the sample CMP05. Eventually, no weight gain occurs in the sample CMP01. All the manganese oxides transform into metastable Mn_2O_3 (bixbyite-C) at ~545 °C regardless of relative amount of manganese species with different oxidation states. Further heat treatment at higher temperatures also makes metastable Mn_2O_3 transform to the high-temperature stable form, Mn_3O_4.[25]

This phase transformation behavior can be utilized to produce Mn_2O_3 with uniform phase and particle morphogy. Figure 8 shows the calcined sample CMP03. The brown color of the powder turns to black when calcined at 550 °C for 1 h. The resulting Mn_2O_3 has cubelike particles of 20 nm size, still maintaining uniformity in particle shape.

V. CONCLUSIONS

The presence and addition sequence of H_2O_2 significantly influence particle characteristics of the synthesized manganese oxides including crystal structure,

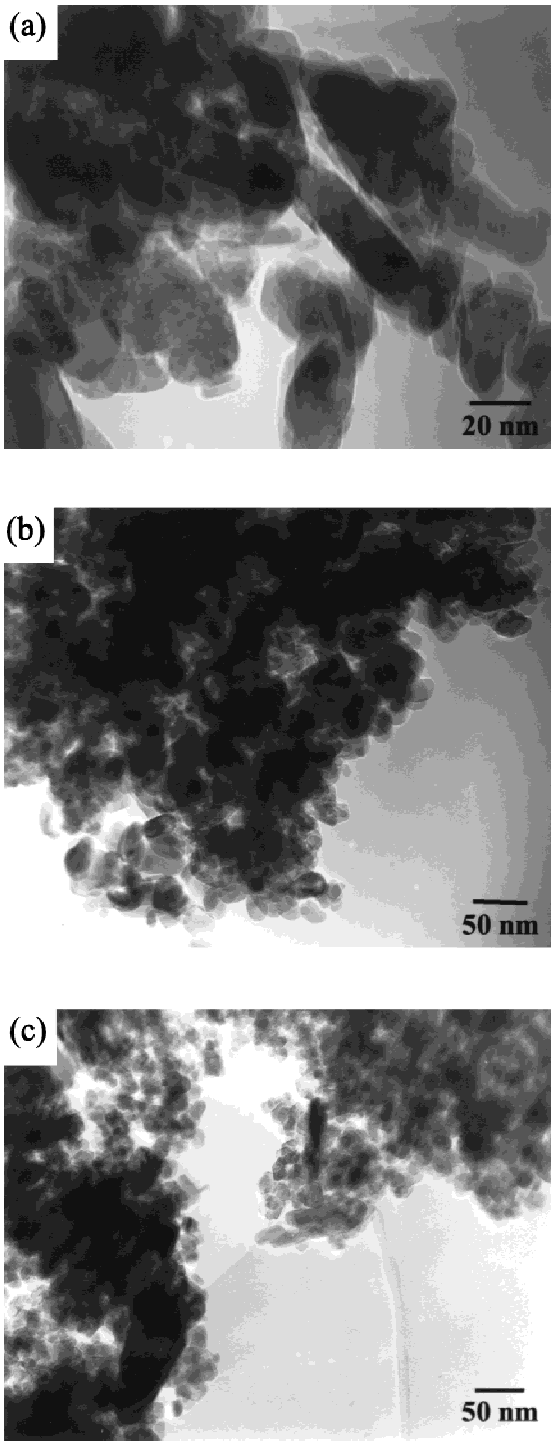

FIG. 7. TEM micrographs showing the influence of precursor concentration on the particle size of Mn_3O_4: (a) 0.1 M, (b) 0.2 M, and (c) 0.4 M.

particle size and morphology, and surface area. X-ray analysis indicated that the precipitation from H_2O_2-added manganese solution resulted in flakelike-shaped amorphous hydrous manganese oxide ($MnO_2 \cdot xH_2O$), whereas amorphous $Mn(OH)_2$ was obtained in the absence of H_2O_2. A portion of amorphous $Mn(OH)_2$ can rapidly crystallize into Mn_3O_4 in alkaline conditions by oxidation in air, and the final precipitate is a mixture of relatively spherical $Mn(OH)_2$ of 80-nm size and cubelike Mn_3O_4 of 14 nm. The post-treatment of these mixed manganese oxides with H_2O_2 modifies phase and particle morphology depending upon molar ratio of H_2O_2 with respect to Mn. It is believed that H_2O_2 preferentially dissolves amorphous $Mn(OH)_2$ at the lower concentration of $Mn:H_2O_2 = 1:1$ and causes additional nucleation and growth of Mn_3O_4 from the solution of Mn^{3+} species. At $Mn:H_2O_2 = 1:4$, the well-defined 16-nm-sized nanocrystalline Mn_3O_4 with homogeneous particle morphology was prepared. The treatment with excess H_2O_2 destroyed crystalline Mn_3O_4, on the other hand, and caused further oxidation of aqueous manganese species, from which needlelike Mn_2O_3 precipitated out. TEM microstructural evidence and thermogravimetrical analysis support our hypothesis of the influences of H_2O_2 post-treatment on the manganese oxide characteristics. The current synthesis approach would find it useful in cost-effective preparation of nanocrystalline Mn_3O_4 and Mn_2O_3 for a variety of applications including catalyst and CMP.

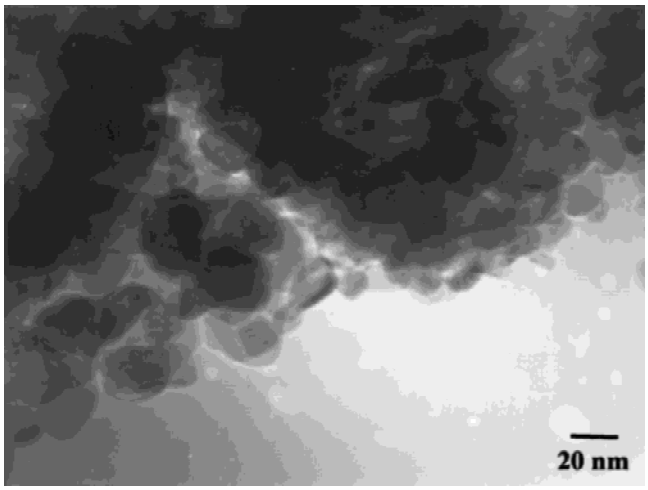

FIG. 8. TEM micrograph of Mn_2O_3 prepared by calcination of the sample CMP03 at 550 °C for 1 h.

REFERENCES

1. T. Yamashita and A. Vannice, J. Catal. **161,** 254 (1996).
2. L. Sanchez, J. Farcy, J-P. Pereira-Ramos, L. Hernan, J. Morales, and J.L. Tirado, J. Mater. Chem. **6,** 37 (1996).
3. V.V. Pankov, Ceram. Int. **14,** 87 (1988).
4. C.H. Hare and M.G. Fernald, Modern Paint Coat. **74,** 40 (1984).
5. T. Hara, T. Tomisawa, T. Kurosu, and T.K. Doy, J. Electrochem. Soc. **146,** 2333 (1999).
6. Y. Arimoto, K. Nakamura, K. Hanawa, A. Hatada, S. Kishii, R. Suzuki, and N. Urda, European Patent No. EP0816457 (7 Jan 1998).

7. K. Hanawa, K. Suzuoka, K. Kato, and T. Sukaue, Boundary **14,** 8 (1998) (in Japanese).
8. G. Zhang, G. Burdick, F. Dai, T. Bibby, and S. Beaudoin, Thin Solid Films **332,** 379 (1998).
9. S.L. Brock, N. Duan, Z.R. Tian, O. Giraldo, H. Zhou, and S.L. Suib, Chem. Mater. **10,** 2619 (1998).
10. S. Bach, M. Henry, N. Baffier, and J. Livage, J. Solid State Chem. **88,** 325 (1990).
11. J. Luo and S.L. Suib, J. Phys. Chem. B **101,** 10403 (1997).
12. Q. Feng, K. Yanagisawa, and N. Yamasaki, J. Porous Mater. **5,** 153 (1998).
13. A. Ardizzone, C.L. Bianchi, and D. Tirelli, Colloid Surf. **134,** 305 (1998).
14. I.U. Haq and E. Matijević, J. Colloid Interface Sci. **192,** 104 (1997).
15. C. Zhiwen, Z. Shuyuan, T. Shun, L. Fanqing, W. Jian, J. Sizhao, and Z. Yuheng, J. Cryst. Growth **180,** 280 (1997).
16. S.B. Kanungo, J. Chem. Tech. Biotechnol. **50,** 91 (1991).
17. Y.P. Liu, Y.T. Qian, Y.H. Zhang, M.W. Zhang, C.S. Wang, and L. Yang, Mater. Res. Bull. **32,** 1055 (1997).
18. N.A. Dhas, Y. Koltypin, and A. Gedanken, Chem. Mater. **9,** 3159 (1998).
19. Z. Weixin, W. Cheng, Z. Xiaoming, X. Yi, and Q. Yitai, Solid State Ionics **117,** 331 (1999).
20. S.B. Kanungo, K.M. Parida, and B.R. Sant, Electrochim. Acta **26,** 1147 (1981).
21. H.W. Nesbitt and D. Banerjee, Am. Mineral. **83,** 305 (1998).
22. S.H.R. Davies and J.J. Morgan, J. Colloid Interface Sci. **129,** 63 (1989).
23. J.W. Murry, J. Colloid Interface Sci. **46,** 357 (1974).
24. S.B. Kanungo, K.M. Parida, and B.R. Sant, Electrochim. Acta **26,** 1157 (1981).
25. S. Fritsch and A. Navrotsky, J. Am. Ceram. Soc. **79,** 1761 (1996).